Applied Catalysis B: Environmental 221 (2018) 312–319

Contents lists available at ScienceDirect

Applied Catalysis B: Environmental

journal homepage: www.elsevier.com/locate/apcatb

Highly efficient visible-light driven photocatalytic reduction of CO_2 over g-C_3N_4 nanosheets/tetra(4-carboxyphenyl)porphyrin iron(III) chloride heterogeneous catalysts

Lin Lin[a,c], Chunchao Hou[b], Xuehua Zhang[a,*], Yanjie Wang[a,c], Yong Chen[b,c,*], Tao He[a,c,*]

[a] CAS Key Laboratory of Nanosystem and Hierarchical Fabrication, CAS Center for Excellence in Nanoscience, National Center for Nanoscience and Technology, Beijing 100190, China

[b] Key Laboratory of Photochemical Conversion and Optoelectronic Materials, Technical Institute of Physics and Chemistry, Chinese Academy of Sciences, Beijing 100190, China

[c] University of Chinese Academy of Sciences, Beijing 100049, China

ARTICLE INFO

Keywords:
CO_2 photoreduction
Visible light
g-C_3N_4 nanosheets
Fe tetra(4-carboxylphenyl)porphyrin chloride
Heterogeneous catalysts

ABSTRACT

Photocatalytic reduction of CO_2 into value-added chemicals is particularly attractive as it could produce renewable energy and capture greenhouse gas. Photoreduction of CO_2 can be realized over molecular and inorganic catalysts. The former usually exhibit high activity, but low stability and often inactive under visible-light irradiation; the latter has low activity, but good stability. Here we use g-C_3N_4 nanosheets as the photosensitizer to integrate with Fe tetra(4-carboxylphenyl)porphyrin chloride (FeTCPP) molecular catalyst. Besides π-π stacking between tri-*s*-triazine unit and porphyrin, the carboxyl group modified Fe porphyrin is used for the first time in CO_2 photoreduction so as to form hydrogen bonding with the rich amino groups in g-C_3N_4 nanosheets. g-C_3N_4/FeTCPP heterogeneous catalysts are prepared via a facile self-assembly approach, in which light harvest is separated from catalysis spatially and temporally. The obtained g-C_3N_4/FeTCPP heterogeneous catalysts exhibit high activity for CO_2 reduction under visible-light irradiation, with CO yield of 6.52 mmol g^{-1} in 6 h and selectivity up to 98%. Fluorescence data indicate that the electrons can efficiently transfer from the g-C_3N_4 nanosheets to FeTCPP. The mechanism for CO_2 reduction over the g-C_3N_4/FeTCPP heterogeneous catalysts is proposed based on the results of quasi in-situ ESR and UV–vis measurements. This work may pave a facile approach for fabricating the high-efficient photocatalysts for CO_2 reduction, as well as better understanding the related mechanism.

1. Introduction

Converting CO_2 into value-added chemicals can mitigate carbon emission and provide alternative energy source [1–3]. Among different approaches, photocatalytic reduction of CO_2 has attracted much interest since late 1970's [4–8]. However, CO_2 reduction is a highly energy demanding process, as formation of $CO_2^{\cdot -}$ via one-electron reduction occurs at a very negative potential ($E_0 = -1.90$ V vs. normal hydrogen electrode (NHE) in solution). The CO_2 reduction can take place via multi-proton-coupled multi-electron reduction reactions, resulting in the formation of many products like CH_4, CH_3OH and CO. The standard redox potential is relatively low for the production of the final products, while with a high overpotential. So the utilization of a catalyst is crucial to initialize and boost the CO_2 photoreduction [9,10].

Metal-based molecular complexes have been employed as homogeneous photocatalysts for CO_2 reduction. Most of them are based on the noble rhenium or ruthenium [11–13], and only few are earth abundant and environmentally benign metals [14,15]. Among them, iron porphyrins play a vital role in catalysis, especially in natural photosynthesis. Robert et al. have used iron porphyrins modified by phenolic group as electro- and/or photo-catalysts to reduce CO_2 to CO with a selectivity > 90% in the homogenous systems [16–20]. It is noted that the molecular catalysts like iron porphyrins suffer from the photodegradation under long-term UV irradiation and most of them are inactive for CO_2 reduction under visible light in case without a photosensitizer [17–19]. Thus, it still remains a big challenge to achieve CO_2 reduction with high efficiency and selectivity over iron porphyrin-based photocatalysts.

One approach to address the aforementioned problems is to incorporate an organic photosensitizer with the iron porphyrin for CO_2

* Corresponding authors.
E-mail addresses: zhangxh@nanoctr.cn (X. Zhang), chenyong@mail.ipc.ac.cn (Y. Chen), het@nanoctr.cn (T. He).

http://dx.doi.org/10.1016/j.apcatb.2017.09.033
Received 27 July 2017; Received in revised form 28 August 2017; Accepted 14 September 2017
Available online 15 September 2017
0926-3373/

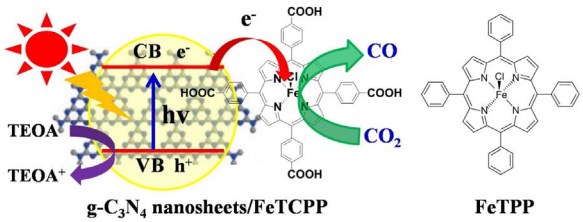

Scheme 1. Structure of g-C_3N_4/FeTCPP heterogeneous catalyst system and FeTPP.

reduction under visible-light irradiation [17]. Considering inorganic materials usually show superior stability to the organic counterparts and exhibit fairly strong light absorption, inorganic nanomaterials can be used as the light absorber to incorporate with the molecular catalysts [21–24]. In this case, the hybrid systems have the strengths of not only high efficiency and selectivity from the molecular catalysts, but also high stability, easy recycling and visible-light activity from the inorganic nanomaterials. More important, the light harvest is separated from catalysis spatially and temporally, resulting in efficient separation and transfer of charge carriers. Graphite carbon nitride (g-C_3N_4) has been studied for various applications by virtue of visible-light absorption, rich marginal amino groups, high stability and earth-abundant nature [25–35], which has also been used as the photosensitizer to incorporate with metal based molecular catalysts [36,37].

Here we have synthesized a carboxyl group modified iron porphyrin catalyst, tetra(4-carboxyphenyl)porphyrin iron(III) chloride (FeTCPP), and fabricated a highly efficient g-C_3N_4 nanosheets/FeTCPP (g-C_3N_4/FeTCPP) heterogeneous catalyst for photoreduction of CO_2 to CO under visible light (Scheme 1). The g-C_3N_4/FeTCPP heterogeneous catalyst was fabricated by integrating FeTCPP with g-C_3N_4 nanosheets via a simple self-assembly approach, in which the cost effective g-C_3N_4 nanosheets act as the light-harvesting unit and environment-friendly iron-based FeTCPP works as the catalytic center. Two molecular catalysts with and without the carboxyl groups, i.e., the FeTCPP and Fe meso-tetraphenylporphine chloride (FeTPP) have been used to study the influence of carboxyl groups. Fairly strong interaction can exist between the g-C_3N_4 nanosheets and FeTCPP via both hydrogen bonding and π-π stacking through the marginal amino groups of g-C_3N_4 nanosheets with the carboxyl groups on FeTCPP and tri-s-triazine units with porphyrins, respectively, which can facilitate the charge transfer between them. More important, the CO_2 reduction mechanism using g-C_3N_4/FeTCPP heterogeneous catalysts is proposed based on the results of quasi in-situ electron spin resonance (ESR) and ultraviolet–visible spectroscopy (UV-vis) measurements. This is the first report that carboxyl-group modified iron porphyrin is employed as the photocatalyst for CO_2 reduction.

2. Experimental

2.1. Chemicals

All of the chemicals and solvents used were analytical grade or chromatographic grade. Dicyandiamide, N,N-dimethylformamide (DMF) and tetraethylammonium tetrafluoroborate (Et_4NBF_4) were obtained from Sigma-Aldrich. N,N-dimethylacetamide (DMA), triethanolamine (TEOA) and acetonitrile (MeCN) were purchased from Shanghai Aladdin Bio-chem Technology. Carbon dioxide gas (super grade purity 99.999%) was bought from Beijing Beiwen Gases Company. FeTPP was purchased from Alfa. Ultrapure water (Millipore Milli-Q grade with a resistivity of 18.2 MΩ cm) was used in all the experiments.

2.2. Synthesis of FeTCPP

Metal-free tetra(4-carboxyphenyl)porphyrin (TCPP) was used as received and the corresponding FeTCPP was synthesized according to previous report [38]. Briefly, FeTCPP was synthesized by refluxing 0.33 mmol of TCPP with 1.82 mmol of $FeCl_3$ in DMF solvent under Ar for 2 h and was monitored by thin layer chromatography analysis. Then, after cooling to room temperature, DMF was removed by distillation and FeTCPP was precipitated by adding excess water. The solid sample was obtained by being dried under vacuum and characterized by high resolution mass spectra (Fig. S1, HR ESI$^+$). $[M\text{-}Cl]^+$ ($C_{48}H_{28}FeN_4O_8$) Calculated: 844.1257; Observed: 844.1258.

2.3. Preparation of g-C_3N_4 nanosheets and g-C_3N_4/FeTCPP heterogeneous catalysts

Bulk g-C_3N_4 was prepared by typical thermal polymerization of dicyandiamide, simply heated 5 g dicyandiamide to 550 °C in muffle furnace with a ramp rate of 2.3 °C min^{-1}, and kept at this temperature for 4 h in ambient atmosphere. The g-C_3N_4 nanosheets were prepared by direct thermal oxidation etching of bulk g-C_3N_4 at 500 °C for 2 h as reported previously [39]. The g-C_3N_4/FeTCPP heterogeneous catalysts were prepared by integrating FeTCPP with g-C_3N_4 nanosheets via a simple self-assembly approach via mechanical mix under stirring.

2.4. Characterization

The morphology of g-C_3N_4 was observed with a Hitachi SU8200 scanning electron microscope (SEM). Transmission electron microscopy (TEM) was operated on a FEI Tecnai G2 T20 electron microscope. Powder X-ray diffraction (XRD) was measured on a Bruker D8 diffract meter with Cu Kα radiation (λ = 0.15406 nm). Nitrogen adsorption–desorption isotherm curves were analyzed on a Micromeritics TriStarII 3020. UV–vis diffuse reflectance spectroscopy (DRS) and UV–vis absorption spectra were recorded on a Lambda 750 UV/Vis/NIR spectrophotometer (Perkin-Elmer, USA). The quasi in-situ UV–vis absorption spectra were measured in a well-sealed quartz cell under visible-light irradiation (Xenon lamp, 420 nm < λ < 780 nm, 220 mW cm^{-2}) with various time (0 min ~ 1 h), the solution (acetonitrile: water: TEOA, 3:1:1, v:v:v) were purged with Ar or CO_2 at least for 1 h before irradiation. Fourier transform-infrared spectra (FT-IR) were recorded on a Spectrum One Spectrometer (Perkin-Elmer, USA).

Photoluminescence (PL) and time-resolved PL decay spectra were collected on a NanoLOG-TCSPC spectrophotometer (Horiba Jobin Yvon, USA) by being excited at 390 nm. ESR measurements were carried out on a JEOL JES-FA-200 spectrometer (JEOL Ltd., Tokyo, Japan), the solution were prepared in DMA and TEOA mixed solution (volume, 4:1) under both Ar and CO_2 atmosphere in dark and with visible-light irradiation (420 nm < λ < 780 nm, 5 min), respectively. Cyclic voltammetry (CV) of the Fe porphyrin complexes was performed in DMF solution containing Et_4NBF_4 (0.1 mol L^{-1}) as the supporting electrolyte with the CHI 660D potentiostat in a standard three-electrode cell at room temperature under Ar or CO_2 atmosphere. Glassy carbon electrode, Pt plate and Ag/AgCl electrode were used as working, counter and reference electrode, respectively. The concentration of the Fe porphyrin catalyst was 1 mmol L^{-1} and the scan rate was 100 mV s^{-1}. Finally the redox potential values were converted to the values vs. normal hydrogen electrode (NHE).

2.5. Photocatalytic reduction of CO_2

The photocatalytic reduction of CO_2 was carried out in a photoreaction system (Labsolar-IIIAG, Beijing Perfectlight Technology Co., Ltd.) saturated with 26 KPa CO_2 at 15 °C as reported previously [5,30]. The g-C_3N_4/FeTCPP heterogeneous catalysts were prepared by mechanical mix of 50 mg g-C_3N_4 nanosheets and different amount (0.1, 0.25, 0.5, 1.0, and 2.0 mg) of FeTCPP in 100 mL solution of acetonitrile/water/TEOA (3:1:1, v:v:v) under stirring. The whole system was vacuumed and purged with Ar for three times to remove the air. The high purity CO_2 gas was bubbled into the quartz reactor for at least 90 min before illumination. The light source (420 nm < λ < 780 nm)

was a 300 W xenon lamp (Microsolar 300, Beijing Perfectlight Technology Co., Ltd.) with a 420 nm cut off filter and an IR-cut filter, the intensity was 220 mW cm^{-2}. The gas products were analyzed by using Agilent 7890A gas chromatography equipped with a hydrogen flame ionized detector (FID) and a thermal conductivity detector (TCD) using He as carrier gas. The FID detector was fitted with a methanizer to detect CO. A series of control experiments (without CO_2 purging, blank solvent without the photocatalysts, dark experiment without illumination, and only the Fe porphyrin) were performed to ensure that the observed products come solely from the photoreduction of CO_2. Turnover number (TON, $mole_{CO}/mole_{FeTCPP}$) was defined as the ratio of the amount of the reduction product CO to the initial amount of introduced Fe porphyrin molecular catalyst.

3. Results and discussion

3.1. Characterization of g-C_3N_4 nanosheets and g-C_3N_4/FeTCPP heterogeneous catalysts

The g-C_3N_4 nanosheets show a morphology with very thin feature compared with bulk g-C_3N_4, and the edge is partially curly due to the ultrathin characteristic (Fig. 1). Such very thin nature can be beneficial to charge transfer longitudinally. The specific surface area of the g-C_3N_4 nanosheets (135.8 $m^2 g^{-1}$) is ~4.5 times of that of the bulk g-C_3N_4 (30.0 $m^2 g^{-1}$) (Fig. S2), indicating effective etching of bulk g-C_3N_4, which can be in favor of the adsorption of FeTCPP on g-C_3N_4. Although no difference can be observed in the SEM and TEM images between the g-C_3N_4 nanosheets and g-C_3N_4/FeTCPP hybrids since FeTCPP is a small organic molecule in nature, the Fe signal can be found in the EDX elemental mapping of g-C_3N_4/FeTCPP hybrids (Fig. S3), suggesting the successful hybridization of g-C_3N_4 nanosheets and FeTCPP. The XRD pattern of g-C_3N_4 nanosheets (Fig. 2a) shows two characteristic peaks of g-C_3N_4 crystal structure at 13.1° and 27.67°, corresponding to the respective plane of (100) and (002) of the periodic stacking lamellar structure of g-C_3N_4. After integration with FeTCPP, the peak angle (002) originated from the periodic stacking of layers in g-C_3N_4 nanosheets is slightly larger than that of pure g-C_3N_4 nanosheets (27.34°) due to the π-π interaction between the g-C_3N_4 nanosheets and FeTCPP through tri-*s*-triazine unit in porphyrin. It can be seen from the UV–vis DRS (Fig. 2b) spectra that both bulk and nanosheet g-C_3N_4 exhibit visible-light absorption, albeit blue shift occurs in the absorption edge

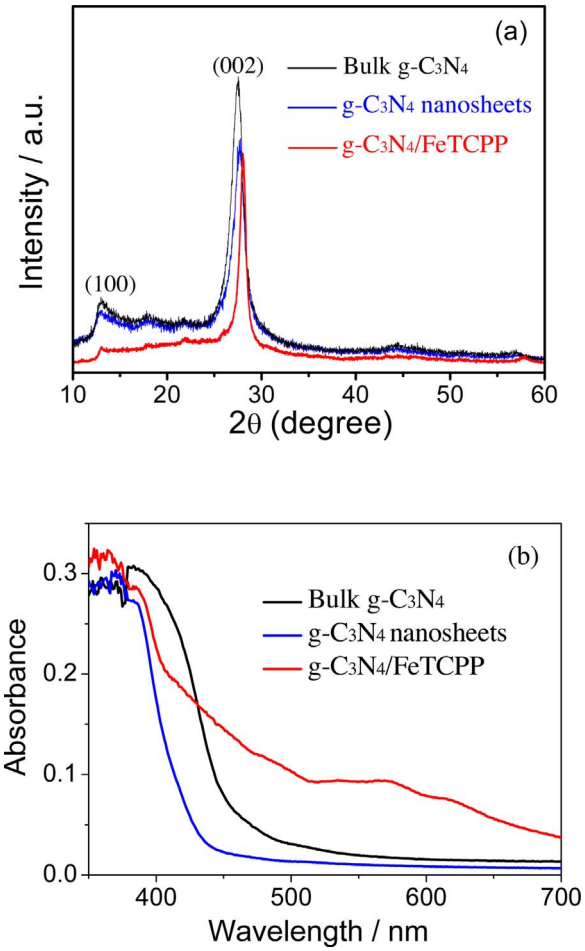

Fig. 2. (a) XRD patterns and (b) UV–vis DRS spectra of the as-prepared bulk g-C_3N_4, g-C_3N_4 nanosheets, g-C_3N_4/FeTCPP hybrids prepared with 50 mg g-C_3N_4 and 2 mg FeTCPP.

of g-C_3N_4 nanosheets (~430 nm) compared with the bulk g-C_3N_4 (~460 nm) due to the quantum confinement effect. In addition, the DRS spectrum of g-C_3N_4/FeTCPP hybrid shows combined absorption

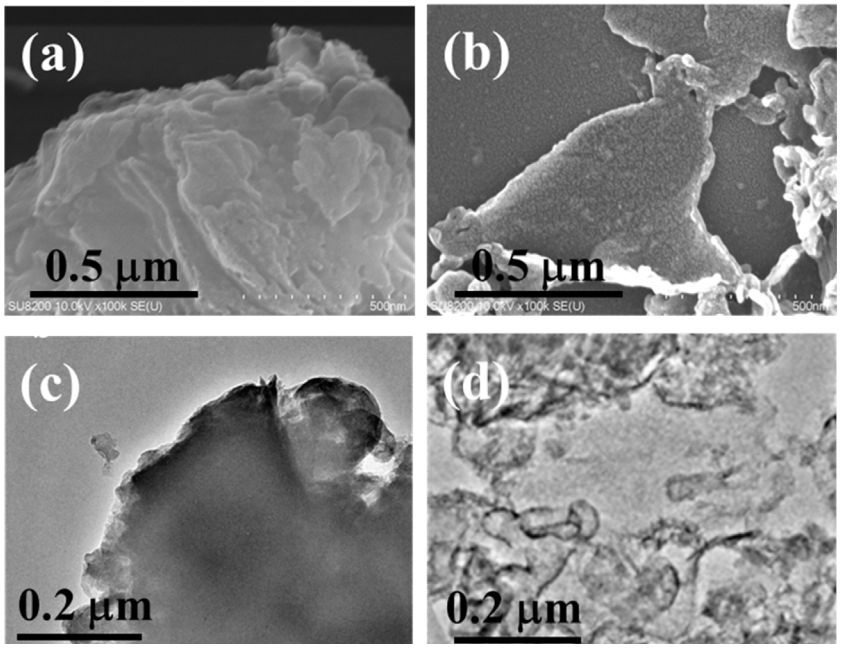

Fig. 1. SEM (a and b) and TEM (c and d) images of (a and c) bulk g-C_3N_4 and (b and d) g-C_3N_4 nanosheets.

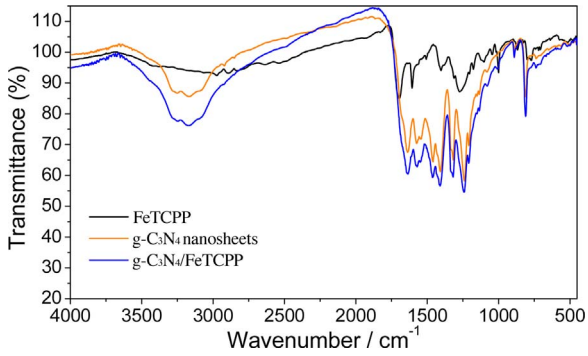

Fig. 3. FT-IR spectra of g-C_3N_4 nanosheets, FeTCPP and g-C_3N_4/FeTCPP hybrids.

feature of both g-C_3N_4 nanosheets and FeTCPP, indicating the successful integration of g-C_3N_4 nanosheets with FeTCPP again.

FT-IR spectra (Fig. 3) were also measured to verify the g-C_3N_4/FeTCPP heterogeneous catalysts. A characteristic peak at 999 cm^{-1} which is ascribed to the Fe-N band appears in the spectra, indicating the formation of a Fe porphyrin compound. The band at 2940 cm^{-1} is assigned to the C—H bond of the benzene and pyrrole rings. The bands at about 1696-1539 and 1380 cm^{-1} are attributed to the C=C stretching mode and C—N stretching vibration, respectively. The bands at about 3415, 1740 and 1204 cm^{-1} are assigned to the O—H, C=O and C—O bonds of carboxyl groups, respectively. These characteristic peaks confirm the successful synthesis of the FeTCPP. It is found that the FT-IR spectra of g-C_3N_4/FeTCPP hybrid keep almost all the major peaks of pure g-C_3N_4, in which the peak at 1638 cm^{-1} is attributable to the C—N heterocycle stretching vibration mode, and the peaks at 1241, 1319 and 1411 cm^{-1} are due to the aromatic C—N stretching. The two main metal-porphyrin characteristic peaks of 1608 and 999 cm^{-1} are present in the g-C_3N_4/FeTCPP hybrid too. The broad peak at 3000–3700 cm^{-1}, corresponding to the unpolymerized N—H vibration of g-C_3N_4, switches to large wavenumber slightly, indicating the possible effect from hydrogen bonding of N—H groups in the g-C_3N_4 with carboxyl groups in the FeTCPP. In addition, it is noted that some peaks of FeTCPP are overlapped with the related strong peaks of g-C_3N_4. Thus, the FT-IR results suggest that fairly strong interactions exist between the g-C_3N_4 nanosheets and FeTCPP via hydrogen bonding and π-π stacking through the marginal amino group in g-C_3N_4 with carboxyl group in FeTCPP and tri-*s*-triazine unit with porphyrin, respectively [40,41].

3.2. Photoreduction of CO_2 over the heterogeneous catalysts

The FeTCPP is inactive under visible-light irradiation in the absence of g-C_3N_4 nanosheets, as no products can be observed in all the control experiments (Table S1). The as-prepared g-C_3N_4/FeTCPP heterogeneous photocatalysts exhibit efficient photocatalytic activity for CO_2 reduction to CO with trace amount of CH_4 under visible-light illumination (420 ~ 780 nm), no H_2 or any other liquid products can be observed within 6 h. It is found that the total CO evolution amount increases with increasing amount of FeTCPP due to increasing quantity of catalytic centers (Fig. 4a), while the CO yield per gram of FeTCPP and the TON value reduce with increasing amount of FeTCPP (Fig. 4b). The latter may be because FeTCPP cannot be fully utilized in case of excess amount, which may even hinder light harvesting since FeTCPP has a strong Soret-band absorption at 428 nm but inactive under visible-light irradiation. The selectivity for CO production can reach as high as above 98%. The CO yield increases linearly in 6 h for all the g-C_3N_4/FeTCPP catalytic systems (Fig. 4a). Moreover, when 50 mg of g-C_3N_4 was used to hybridize with 0.1 mg of FeTCPP, the CO yield increases almost linearly within 12 h (Fig. S5). Thus, stability of the obtained g-C_3N_4/FeTCPP hybrid catalysts is relatively good under visible-light irradiation. In this case, the yield can reach as high as 1.09 mmol per gram of FeTCPP per hour and the corresponding value of TON is 5.7

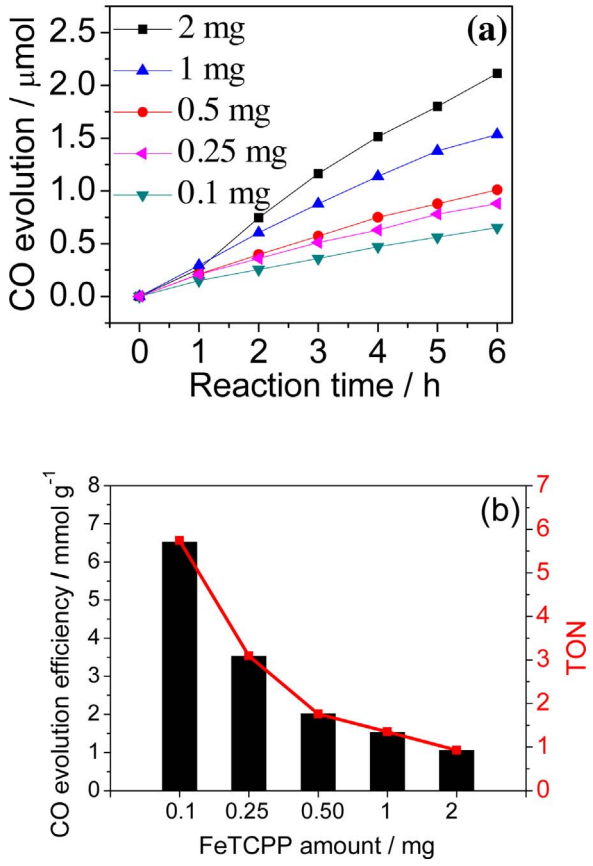

Fig. 4. Dependence of (a) total CO evolution amount and (b) CO evolution amount per gram of FeTCPP (mmol g^{-1}) (column chart) and the TON (linear) within 6 h with the amount of FeTCPP (0.10, 0.25, 0.50, 1.0 and 2.0 mg) and 50 mg of g-C_3N_4 nanosheets in CH_3CN:H_2O:TEOA (3:1:1, 100 mL) mixed solution under visible-light illumination (420 nm < λ < 780 nm), light intensity = 220 mW cm^{-2}.

in 6 h.

In addition, the iron porphyrin without carboxyl groups, i.e., FeTPP (Scheme 1), was used to study the effect of carboxyl group. It is found that the g-C_3N_4/FeTPP photocatalyst shows very low activity for CO_2 photoreduction (Fig. S4). So the introduction of carboxyl groups in the molecular catalysts can lead to considerable increase in the catalytic activity. The surface of g-C_3N_4 nanosheets is terminated with plenty of amino groups that can form hydrogen bonds with the carboxyl groups, enhancing interaction between FeTCPP and g-C_3N_4 and, thus, promoting the electron transfer. Another reason is that the FeTCPP is more prone to accepting electrons from g-C_3N_4 nanosheets than FeTPP, as the E^0 values of $Fe^{III}/Fe^{II}/Fe^{I}/Fe^0$ redox couples for FeTCPP are more positive or less negative than those of FeTPP since the four carboxyl groups on the para position of phenyl rings in FeTCPP exhibit electron-withdrawing property in nature. The values of $E^0_{Fe}{}^{III/II}$, $E^0_{Fe}{}^{II/I}$ and $E^0_{Fe}{}^{I/0}$ are measured to be 0.028, −0.84 and −1.40 V (vs. NHE) for FeTPP in DMF solution after being purged with Ar, and 0.031, −0.61 and −1.30 V for FeTCPP. The above redox potentials shift slightly to the positive pole when the solution is saturated with CO_2 instead of Ar, i.e., 0.32, −0.53 and −1.14 V for FeTPP, and 0.33, −0.49 and −1.02 V for FeTCPP, respectively. However, it is noted that the real redox potential would be marginally different from those measured in DMF, as the CO_2 reduction was undergone in a mixed solution of acetonitrile, water and TEOA.

It is noted that only little amount of CH_4 (0.28 mmol g^{-1}) is observed if just using g-C_3N_4 nanosheets as the catalyst (Table S1). So the observed high yield of CO over the hybrid catalysts has to be related to the integration of g-C_3N_4 and FeTCPP. Considering the conduction band potential of the g-C_3N_4 nanosheets is about −1.25 V (vs. NHE) [39], it

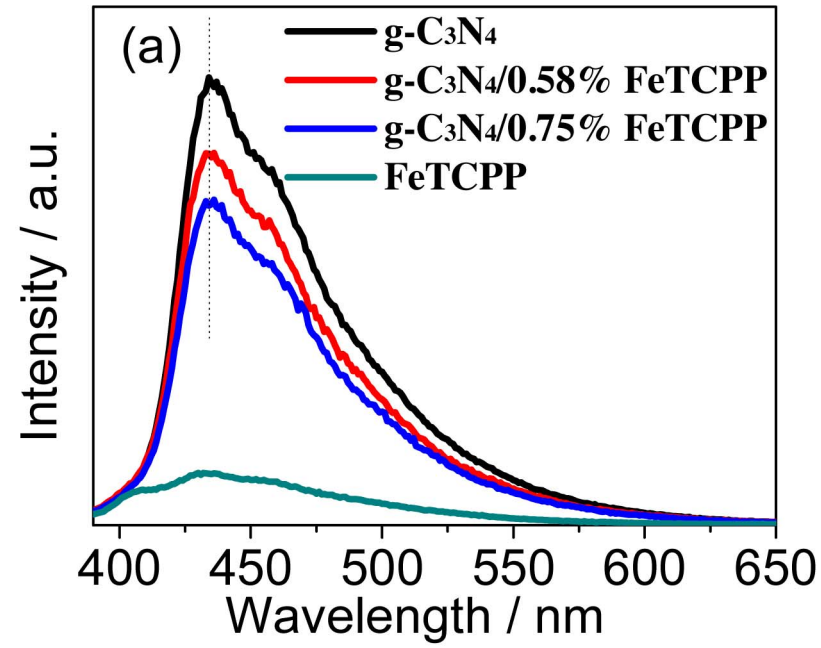

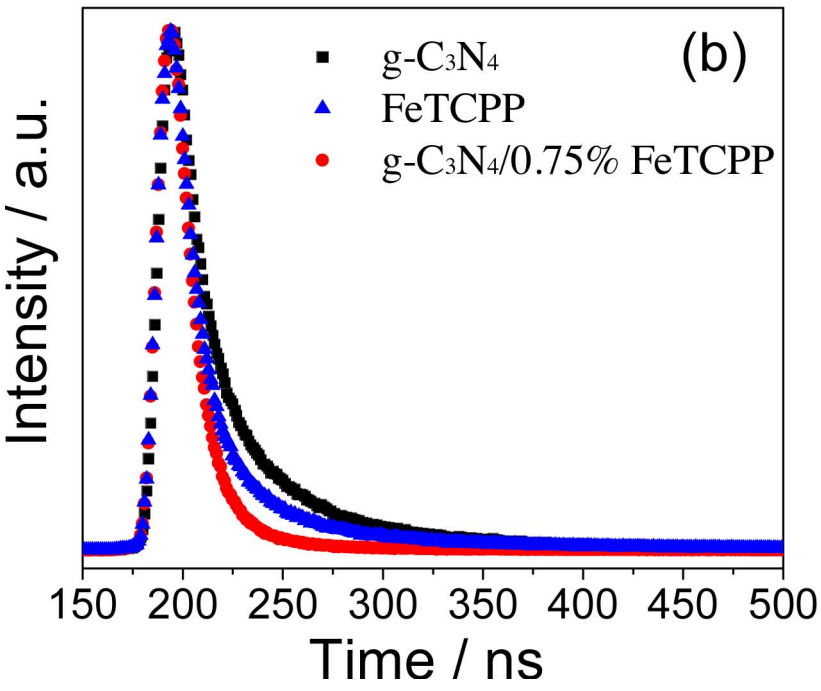

Fig. 5. (a) PL spectra and (b) time-resolved PL decay curves of g-C_3N_4 nanosheets, FeTCPP, and g-C_3N_4/FeTCPP hybrids.

is possible for the electrons to transfer from g-C_3N_4 nanosheets to FeTCPP, i.e., g-C_3N_4 nanosheets act as the light harvesting unit in the heterogeneous system and FeTCPP works as the catalytic center for CO_2 reduction.

3.3. PL and time-resolved PL decay characteristics

PL spectra were measured to verify the charge transfer. The g-C_3N_4 nanosheets exhibit strong PL signal at 434 nm, while the FeTCPP has very weak PL response (Fig. 5a). It is found that the PL signal of the g-C_3N_4 nanosheets can be quenched to some degree by adding FeTCPP, indicating decreased recombination of charge carriers. Thus, the electron can transfer from the g-C_3N_4 nanosheets to FeTCPP. The time-resolved PL decay spectra can further confirm this. Both the g-C_3N_4 nanosheets and g-C_3N_4/FeTCPP hybrid display exponential decay characteristics (Fig. 5b), while g-C_3N_4 nanosheets show slower decay kinetics compared to the g-C_3N_4/FeTCPP. The decay curves can be fitted by using the tri-exponential decay kinetics (Eq. S1). The average lifetime (τ) obtained for g-C_3N_4 nanosheets and g-C_3N_4/FeTCPP is 7.07 and 2.19 ns, respectively, implying the presence of an additional non-radiative decay channel via the electron transfer from g-C_3N_4 nanosheets to FeTCPP [42], while it is noted that the lifetime for such electron transfer is much faster, far beyond the nanosecond scale [24], which cannot be determined here. The lifetime τ is contributed by three different processes, the non-radiative process (τ_1), radiative process (τ_2) that is directly related to the recombination of electrons and holes, and energy transfer process (τ_3). Both the processes of τ_1 and τ_2 are mainly contributed by the g-C_3N_4, as the FeTCPP exhibits very low PL

Table 1
The fitted parameters of fluorescence lifetime for g-C_3N_4 nanosheets and g-C_3N_4/FeTCPP heterogeneous system.

Sample	τ_1/ns (rel.%)	τ_2/ns (rel.%)	τ_3/ns (rel.%)	τ/ns
g-C_3N_4	5.82 (52.16)	1.66 (36.42)	30.04 (11.42)	7.07
g-C_3N_4/FeTCPP	1.29 (84.41)	4.21 (12.50)	18.81 (3.08)	2.19
FeTCPP	5.59 (38.47)	26.20 (11.40)	1.47 (50.73)	5.87

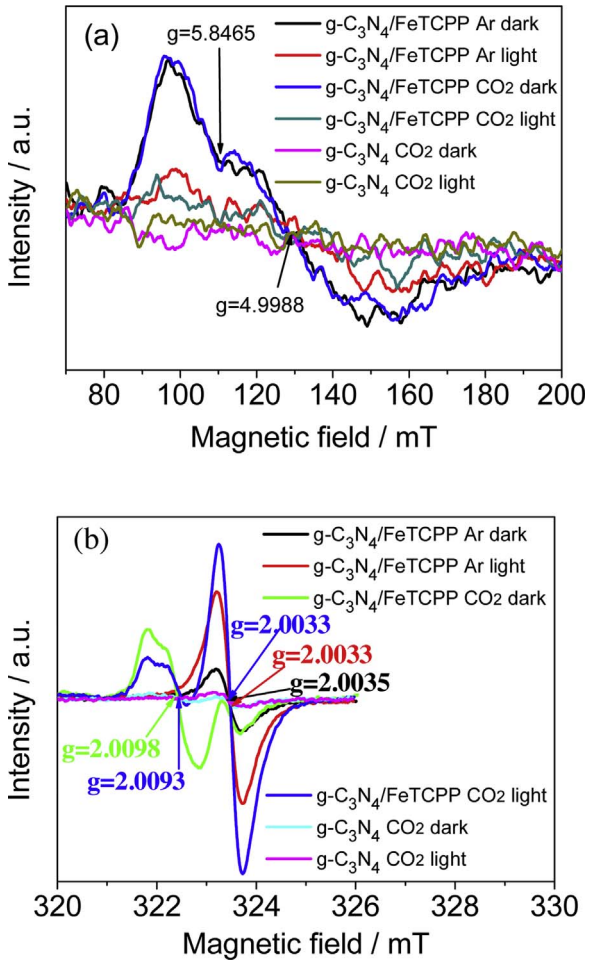

Fig. 6. Quasi in-situ ESR spectra of g-C_3N_4/FeTCPP and pure g-C_3N_4 nanosheets in Ar and CO_2 atmosphere under dark and visible-light irradiation (420 nm < λ < 780 nm), respectively, (a) low field part, (b) high field part.

performance. The g-C_3N_4/FeTCPP exhibits shorter τ_1 but with larger percentage than g-C_3N_4 itself (Table 1), suggesting enhanced transfer of photo-induced electrons from g-C_3N_4 to FeTCPP. In addition, the g-C_3N_4/FeTCPP shows longer τ_2 but with less percentage than g-C_3N_4, indicating a longer lifetime and less recombination for the hybrid.

3.4. Quasi in-situ ESR characteristics

Quasi in-situ ESR measurements for the g-C_3N_4/FeTCPP hybrid and g-C_3N_4 nanosheets were performed to probe catalytic mechanism. The broad resonance at g values of 5.8465 and 4.9988 (Fig. 6a) and the intense peak at around 2.0035 (Fig. 6b) are the characteristic signals of the high spin Fe^{III} tetraphenylporphyrin [43–45]. The photogenerated electrons in g-C_3N_4 nanosheets upon irradiation transfer to Fe^{III}TCPP, leading to the formation of Fe^{II}, Fe^{I}, and Fe^{0} TCPP intermediates. The Fe^{II} and Fe^{0} TCPP give rise to no ESR signal, while the Fe^{I}TCPP has only one intense narrow signal at near g = 2.0033 with slightly anisotropic. Thus, the signals of Fe^{III}TCPP decrease significantly under both Ar and

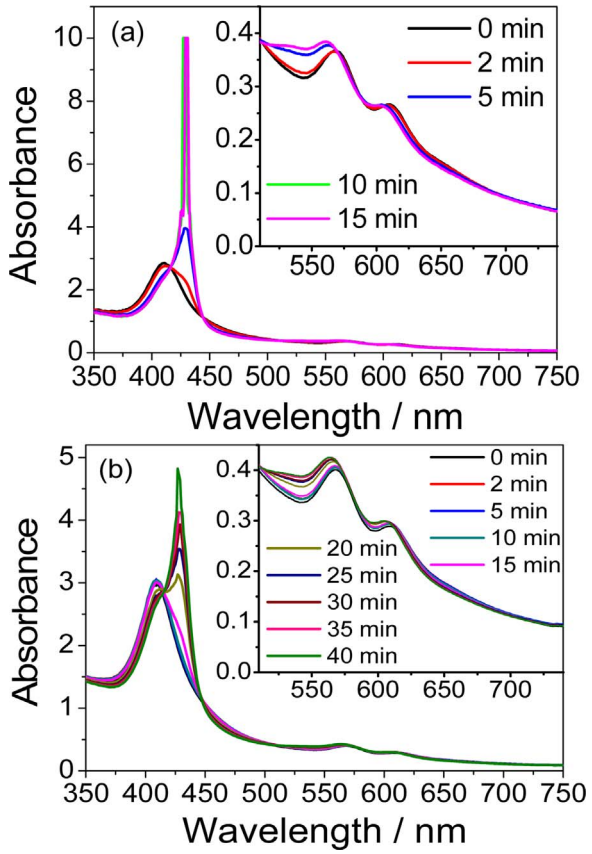

Fig. 7. Quasi in-situ UV–vis absorption spectra of g-C_3N_4/FeTCPP hybrids under visible-light irradiation, (a) purged with Ar, (b) purged with CO_2.

CO_2 atmosphere. The formation of Fe^{I}TCPP intermediate upon irradiation can be manifested by the peak at around g = 2.0033 as shown in Fig. 6b, which increases the most under CO_2 atmosphere. In addition, the signal at around g = 2.009 is attributed to the CO_2 adsorption.

3.5. Quasi in-situ UV–vis absorption characteristics

Quasi in-situ UV–vis absorption spectra were carried out to further study the mechanism. The FeTCPP shows characteristic absorption bands at 410 (Soret band), 568 and 610 nm (Q band) in the visible-light region, corresponding to the Fe^{III} porphyrin state. It is noted that all the states of FeTCPP (Fe^{III}, Fe^{II} and Fe^{I}) have the Soret and Q bands in visible region, leading to inevitable spectral overlap [18,19].

The peak intensity at 410 nm declines slightly for the g-C_3N_4/FeTCPP hybrid under visible-light irradiation in Ar atmosphere (Fig. 7a). Meanwhile, a new peak evolves at 428 nm, which is attributed to Fe^{II}TCPP (Soret band) due to the conversion of Fe^{III} to Fe^{II} and its intensity increases greatly upon irradiation. Moreover, two more new bands appear at 533 and 649 nm after 5-min irradiation, which is ascribed to Fe^{II}TCPP and Fe^{I}TCPP (Q band), respectively, due to the conversion of Fe^{III} to Fe^{II} and Fe^{I} states [46]. Accordingly, the Q bands at 568 and 610 nm for Fe^{III}TCPP blue-shift to 561 and 605 nm, respectively. In addition, the Fe^{0} state cannot be observed due to the very short lifetime of Fe^{0} porphyrin intermediate.

The quasi in-situ absorption spectra under CO_2 atmosphere show a different change trend from that in Ar under visible-light irradiation for the first 15 min (Fig. 7b). The peak at 410 nm blue shifts slightly with a tiny increase in intensity, indicating the formation of Fe^{II}TCPP···CO_2 complex. Meanwhile, like that in Ar, a new peak appears at 428 nm, but it increases very slowly in the beginning. The peak intensity at 410 nm starts to decrease after being irradiated for about 15 min. Though the absorption at 428 nm begins to increase faster simultaneously, the

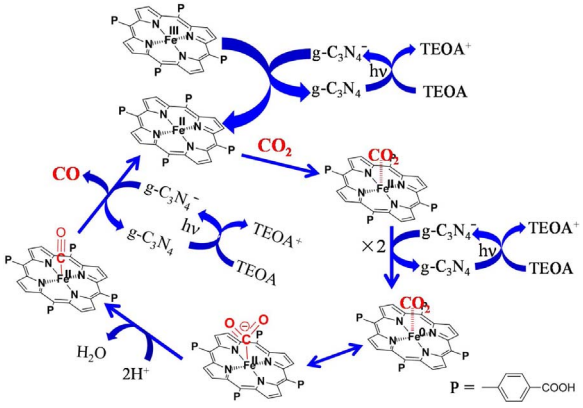

Scheme 2. Proposed catalytic mechanism for CO_2 photoreduction using g-C_3N_4/FeTCPP heterogeneous catalyst with TEOA as sacrificial agent.

increase speed is much slower than that in Ar. Similarly, like those in Ar, two more new peaks evolve at 528 and 649 nm, and the Q bands at 568 and 610 nm blue-shift to 564 and 605 nm, respectively. All these strongly point toward the conversion of Fe^{III} to Fe^{II} and Fe^{I} states. Moreover, the observed slow evolution of low oxidation state of FeTCPP intermediates can be ascribed to the ongoing photoreduction of CO_2 by Fe^0 states [47]. As expected, in addition, almost no changes can be observed in the spectra upon visible-light irradiation if only FeTCPP is present in the solution, even with presence of CO_2 (Fig. S6), indicating it is difficult for the low oxidation state of Fe porphyrins to be formed without g-C_3N_4. So the quasi in-situ UV–vis absorption spectra can well elucidate the evolution of Fe^{II} and Fe^{I} porphyrin intermediates, proving the effective electron transfer from the g-C_3N_4 nanosheets to FeTCPP and the formation of $Fe^{II}TCPP\cdots CO_2$ complex upon irradiation. It is noted that $Fe^{III}TCPP\cdots CO_2$ is not formed, as no aforementioned signal can be detected in the absorption spectrum of Fe^{III}TCPP or Fe^{III}TPP measured with CO_2 (Fig. S6 and S7).

3.6. Mechanism for CO_2 photoreduction over g-C_3N_4/FeTCPP catalysts

The mechanism for CO_2 photoreduction over g-C_3N_4/FeTCPP heterogeneous catalysts can be proposed based on the above results (Scheme 2). The photo-induced electrons in g-C_3N_4 nanosheets first transfer to Fe^{III}TCPP upon irradiation, leading to the formation of Fe^{II}TCPP [Eq. (1, 2)]. Meanwhile, the holes left in g-C_3N_4 nanosheets are harvested by the sacrificial agent TEOA [Eq. (3)]. The [Fe^{II}TCPP$\cdots CO_2$] complex intermediate is formed if CO_2 co-exists in the solution [Eq. (4)], which can further receive electrons from g-C_3N_4 nanosheets, forming $[Fe^{I}TCPP\cdots CO_2]^-$ and $[Fe^{0}TCPP\cdots CO_2]^{2-}$ in sequence [Eq. (5, 6)]. Finally, the catalytically active Fe^0TCPP state will reduce CO_2 to form CO, coupled with proton transfer [Eq. (7–9)]. The re-generation of Fe^{II}TCPP will close the catalytic cycle. Compared with the FeTPP, the carboxyl groups of FeTCPP can stabilize the above CO_2 adduct complexes by intramolecular hydrogen bonds, like phenol groups reported previously [16].

It is noted that the mechanism proposed here is slightly different from that reported in the literature (Fig. S8), which was drawn based on the electrochemical reduction mechanism [18,47]. The generation of active Fe^0 species, Fe-CO_2 adducts and CO is very efficient and fast in the electrochemical reduction. The Fe(0) porphyrin can bind to CO_2 efficiently, forming Fe-CO_2 adduct (i.e., Fe^{II}-CO_2^{2-} intermediate species). The CO bond cleavage may then occur by protonation of the Fe-CO_2 adduct, leading to the release of a water molecule and Fe-CO adduct. The latter further gives rise to CO either upon photoirradiation and/or via one electron reduction by the Fe(0) species (Fig. S8). However, the formation of Fe^0 species is much slower under the heterogeneous photochemical conditions. Since the Fe^{II} and Fe^{I} species do accumulate in the solution for several minutes, as evidenced by the above quasi in-situ ESR and UV–vis results, the formation of the [$Fe^{II}TCPP\cdots CO_2$] complex intermediate may be crucial and take precedence for the CO_2 photoreduction in the reported system here.

4. Conclusions

In summary, we prepared a highly efficient g-C_3N_4/FeTCPP heterogeneous catalyst via a facile self-assembly approach by mechanical mix under stirring for selective photoreduction of CO_2 into CO under visible-light irradiation using cost effective g-C_3N_4 nanosheets as light absorber and abundant environment friendly FeTCPP as catalytic center. The photoinduced electrons in g-C_3N_4 nanosheets can efficiently transfer to FeTCPP. A maximum rate of 6.52 mmol g^{-1} in 6 h and selectivity up to 98% for CO production can be achieved using g-C_3N_4/FeTCPP heterogeneous catalyst. The catalytic photoreduction of CO_2 includes photoexcitation of g-C_3N_4 nanosheets, charge transfer from g-C_3N_4 nanosheets to FeTCPP, formation of Fe^{II}TCPP, [$Fe^{II}TCPP\cdots CO_2$], $[Fe^{I}TCPP\cdots CO_2]^-$ and $[Fe^{0}TCPP\cdots CO_2]^{2-}$ intermediates. Moreover, the carboxyl substituent in the phenyl ring can enhance the interaction between g-C_3N_4 nanosheets and FeTCPP and stabilize CO_2 adduct formed with FeTCPP via intramolecular hydrogen bonding and, thus, improving photocatalytic activity of the g-C_3N_4/FeTCPP heterogeneous catalysts for CO_2 reduction.

Acknowledgements

This work was supported by the National Natural Science Foundation of China (21673052), the Ministry of Science and Technology of China (2015DFG62610, 2013CB834800), and the Strategic Priority Research Program of the Chinese Academy of Sciences (XDB17030300).

Appendix A. Supplementary data

Supplementary data associated with this article can be found, in the online version, at http://dx.doi.org/10.1016/j.apcatb.2017.09.033.

References

[1] Q. Shen, J. Ma, X.F. Huang, N.J. Yang, G.H. Zhao, Appl. Catal. B: Environ. 219 (2017) 45–52.
[2] Y.J. Jang, J. Jang, J. Lee, J.H. Kim, H. Kumagai, J. Lee, T. Minegishi, J. Kubota, K. Domen, J.S. Lee, Energy Environ. Sci. 8 (2015) 3597–3604.
[3] Q. Kang, T. Wang, P. Li, L.Q. Liu, K. Chang, M. Li, J.H. Ye, Angew. Chem. Int. Ed. 54 (2015) 841–845.
[4] T. Inoue, A. Fujishima, S. Konishi, K. Honda, Nature 277 (1979) 637–638.
[5] M.F. Ehsan, T. He, Appl. Catal. B: Environ. 166–167 (2015) 345–352.
[6] X. Li, J.Q. Wen, J.X. Low, Y.P. Fang, J.G. Yu, Sci. China Mater. 57 (2014) 70–100.
[7] J.J. Shan, F. Raziq, M. Humayun, W. Zhou, Y. Qu, G.F. Wang, Y.D. Li, Appl. Catal. B: Environ. 219 (2017) 10–17.
[8] X.X. Chang, T. Wang, J.L. Gong, Energy Environ. Sci. 9 (2016) 2177–2196.
[9] W.G. Tu, Y. Zhou, Z.G. Zou, Adv. Mater. 26 (2014) 4607–4626.
[10] K. Li, B. Peng, T.Y. Peng, ACS Catal. 6 (2016) 7485–7527.
[11] A.J. Morris, G.J. Meyer, E. Fujita, Acc. Chem. Res. 42 (2009) 1983–1994.
[12] H. Takeda, K. Koike, H. Inoue, O. Ishitani, J. Am. Chem. Soc. 130 (2008) 2023–2031.
[13] Y. Kou, Y. Nabetani, D. Masui, T. Shimada, S. Takagi, H. Tachibana, H. Inoue, J. Am. Chem. Soc. 136 (2014) 6021–6030.
[14] H. Takeda, C. Cometto, O. Ishitani, M. Robert, ACS Catal. 7 (2017) 70–88.
[15] T. Ouyang, H.H. Huang, J.W. Wang, D.C. Zhong, T.B. Lu, Angew. Chem. Int. Ed. 56 (2017) 738–743.
[16] C. Costentin, S. Drouet, M. Robert, J.M. Savéant, Science 338 (2012) 90–94.
[17] J. Bonin, M. Robert, M. Routier, J. Am. Chem. Soc. 136 (2014) 16768–16771.
[18] J. Bonin, A. Maurin, M. Robert, Coord. Chem. Rev. 334 (2017) 184–198.
[19] J. Bonin, M. Chaussemier, M. Robert, M. Routier, ChemCatChem 6 (2014) 3200–3207.
[20] H. Rao, J. Bonin, M. Robert, Chem. Commun. 53 (2017) 2830–2833.
[21] X. Liu, S.J. Inagaki, J.L. Gong, Angew. Chem. Int. Ed. 55 (2016) 14924–14950.
[22] S. Sato, T. Morikawa, S. Saeki, T. Kajino, T. Motohiro, Angew. Chem. Int. Ed. 49 (2010) 5101–5105.
[23] M.F. Kuehnel, K.L. Orchard, K.E. Dalle, E. Reisner, J. Am. Chem. Soc. 139 (2017) 7217–7223.
[24] S. Lian, M.S. Kodaimati, D.S. Dolzhnikov, R. Calzada, E.A. Weiss, J. Am. Chem. Soc. 139 (2017) 8931–8938.

[25] X.C. Wang, K. Maeda, A. Thomas, K. Takanabe, G. Xin, J.M. Carlsson, K. Domen, M. Antonietti, Nat. Mater. 8 (2009) 76–80.
[26] D.J. Martin, K.P. Qiu, S.A. Shevlin, A.D. Handoko, X.W. Chen, Z.X. Guo, J.W. Tang, Angew. Chem. Int. Ed. 53 (2014) 9240–9245.
[27] W.J. Ong, L.L. Tan, Y.H. Ng, S.T. Yong, S.P. Chai, Chem. Rev. 116 (2016) 7159.
[28] S.W. Cao, J.G. Yu, J. Phys. Chem. Lett. 5 (2014) 2101–2107.
[29] H.J. Yu, R. Shi, Y.X. Zhao, T. Bian, Y.F. Zhao, C. Zhou, G.I.N. Waterhouse, L.Z. Wu, C.H. Tung, T.R. Zhang, Adv. Mater. 29 (2017) 1605148.
[30] Y. Huang, Y. Wang, Y. Bi, J. Jin, M.F. Ehsan, M. Fu, T. He, RSC Adv. 5 (2015) 33254–33261.
[31] Z.X. Sun, J.M.T.A. Fischer, Q. Li, J. Hu, Q.J. Tang, H.Q. Wang, Z.B. Wu, M. Hankel, D.J. Searles, L.Z. Wang, Appl. Catal. B: Environ. 218 (2017) 672–678.
[32] S.W. Cao, X.F. Liu, Y.P. Yuan, Z.Y. Zhang, Y.S. Liao, J. Fang, S.C.J. Loo, T.C. Sum, C. Xue, Appl. Catal. B: Environ. 147 (2014) 940–946.
[33] M. Zhang, W.J. Jiang, D. Liu, J. Wang, Y.F. Liu, Y.Y. Zhu, Y.F. Zhu, Appl. Catal. B: Environ. 183 (2016) 263–268.
[34] F. Dong, Z.W. Zhao, T. Xiong, Z.L. Ni, W.D. Zhang, Y.J. Sun, W.K. Ho, ACS Appl. Mater. Interfaces 5 (2013) 11392–11401.
[35] S.W. Liu, F. Chen, S.T. Li, X.X. Peng, Y. Xiong, Appl. Catal. B: Environ. 211 (2017) 1–10.
[36] R. Kuriki, K. Sekizawa, O. Ishitani, K. Maeda, Angew. Chem. Int. Ed. 54 (2015) 2406–2409.
[37] G.X. Zhao, H. Pang, G.G. Liu, P. Lia, H.M. Liu, H.B. Zhang, L. Shi, J.H. Ye, Appl. Catal. B: Environ. 200 (2017) 141–149.
[38] G. Granados-Oliveros, E.A. Páez-Mozo, F.M. Ortega, C. Ferronato, J.-M. Chovelon, Appl. Catal. B: Environ. 89 (2009) 448–454.
[39] P. Niu, L. Zhang, G. Liu, H.M. Cheng, Adv. Funct. Mater. 22 (2012) 4763–4770.
[40] A. Fidalgo-Marijuan, G. Barandika, B. Bazán, M.K. Urtiaga, M.I. Arriortua, Polyhedron 30 (2011) 2711–2716.
[41] D. Chen, K. Wang, W. Hong, R. Zong, W. Yao, Y. Zhu, Appl. Catal. B: Environ. 166–167 (2015) 366–373.
[42] W.G. Tu, Y. Zhou, Q. Liu, S.C. Yan, S.S. Bao, X.Y. Wang, M. Xiao, Z.G. Zou, Adv. Funct. Mater. 23 (2013) 1743–1749.
[43] K.C. Christoforidis, M. Louloudi, E.R. Milaeva, Y. Sanakis, Y. Deligiannakism, Mol. Phys. 105 (2007) 105.
[44] C.M.C.P. Manso, C.R. Neri, E.A. Vidoto, H.C. Sacco, K.J. Ciuffi, L.S. Iwamoto, Y. Iamamoto, O.R. Nascimento, O.A. Serra, J. Inorg. Biochem. 73 (1999) 85–92.
[45] C. Bernard, Y.L. Mest, J.P. Gisselbrecht, Inorg. Chem. 37 (1998) 181–190.
[46] J. Grodkowski, D. Behar, P. Neta, P. Hambright, J. Phys. Chem. A 101 (1997) 248–254.
[47] M. Hammouche, D. Lexa, M. Momenteau, J.-M. Savëant, J. Am. Chem. Soc. 113 (1991) 8455–8466.